Proceedings of the 9th International Conference on Energy Sustainability
ES2015
June 28 – July 2, 2015, San Diego, California, USA

PowerEnergy2015-49464

STRUCTURAL ANALYSIS OF A DIRECT HEATED TUBULAR SOLAR RECEIVER FOR SUPERCRITICAL CO_2 BRAYTON CYCLE

Jesus D. Ortega
Sandia National Laboratories, Concentrating Solar Technologies Department
Albuquerque, NM 87185-1127, USA.

Joshua M. Christian
Sandia National Laboratories, Concentrating Solar Technologies Department
Albuquerque, NM 87185-1127, USA.

Clifford K. Ho
Sandia National Laboratories,
Concentrating Solar Technologies Department
Albuquerque, NM 87185-1127,
USA.

ABSTRACT

Closed-loop super-critical carbon dioxide (sCO_2) Brayton cycles are being evaluated in combination with concentrating solar power to provide higher thermal-to-electric conversion efficiencies relative to conventional steam Rankine cycles. However, high temperatures (650 - 700°C) and pressures (20 – 25 MPa) are required in the solar receiver. In this study, an extensive material review was performed along with a tube size optimization following the ASME Boiler and Pressure Vessel Code and B31.1 and B313.3 codes respectively. Subsequently, a thermal-structural model was developed using ANSYS Fluent and Structural to design and analyze the tubular receiver that could provide the heat input for a ~2 MW_{th} plant. The receiver will be required to provide an outlet temperature of 650°C (at 25 MPa) or 700°C (at 20 MPa). The induced thermal stresses were applied using a temperature gradient throughout the tube while a constant pressure load was applied on the inner wall. The resulting stresses have been validated analytically using constant surface temperatures. The cyclic loading analysis was performed using the Larson-Miller creep model in nCode Design Life to define the structural integrity of the receiver over the desired lifetime of ~10,000 cycles. The results have shown that the stresses induced by the thermal and pressure load can be withstood by the tubes selected. The creep-fatigue analysis displayed the damage accumulation due to the cycling and the permanent deformation of the tubes. Nonetheless, they are able to support the required lifetime. As a result, a complete model to verify the structural integrity and thermal performance of a high temperature and pressure receiver has been developed. This work will serve as reference for future design and evaluation of future direct and indirect tubular receivers.

INTRODUCTION

By following Carnot's theorem, the method to improve the solar-to-electric conversion efficiency of a concentrating solar power (CSP) plant is to increase the upper temperature of the thermal power cycle. The power tower technology is considered one of the best options to achieve the temperatures required to produce high-efficiency utility-scale power cycle technologies [1]. Common design of cavity and external receivers are tube-type receivers using tubes to absorb the highly concentrated solar energy and transmit the energy to the heat transfer fluid, such as water/steam, steam, molten salt or air [2-5]. Current superheated and supercritical steam power cycles are capable of achieving thermal efficiencies of the order of 30-40% [6].

Recent studies have evaluated closed-loop supercritical carbon dioxide (sCO_2) Brayton cycles to be a higher energy-density system in comparison to conventional steam Rankine systems [7-11]. Thermodynamic efficiencies ~50% at concentrations and temperatures achievable by solar power towers, [7-13] make the sCO_2 Brayton cycle a viable alternative for the advancement of the CSP technologies. On the other hand, carbon dioxide (CO_2) has a moderate critical pressure, its chemical stability and relative inertness, sufficient knowledge of its thermodynamic properties, non-toxicity, abundance and low cost are some of the reasons why sCO_2 has been proposed lately to be used as a heat transfer fluid in CSP systems [9, 14,

15]. Neises et al. presents an analytical methodology to approximate the stress distributions throughout the tube [1]. As a difference, this paper evaluates the structural design and creep-fatigue analyses of two sCO_2 receiver tubes with operating conditions of 490-650°C (at 25 MPa) or 540-700°C (at 20 MPa).

METHODOLOGY

The *ASME Boiler & Pressure Vessel Code (BPVC)* provides the rules for the design, fabrication, and maintenance of fired and unfired pressure vessels [16-17]. It also provides a wide range of methods for high temperature and high pressure applications, the design criteria focuses mainly on traditional (e.g. coal-fired) boilers and superheaters, which are related, but not similar to CSP receivers [16].

Material Selection

The *ASME BPVC Section II Part D* provides the maximum allowable stress levels at a constant temperature. Nevertheless, these values correspond to the 80% of the minimum creep rupture stress at 100,000 hours. This safety factor of 1.25 is applied to all pressurized vessels. For a working temperature range of 700-800°C, Haynes 230 was selected for the analyses, even though it does not show the highest allowable stresses for the desired temperature range, the oxidation resistance at high temperatures [22]. Figure 1 shows a comparison of Haynes 230 to common alloys used for solar power receivers.

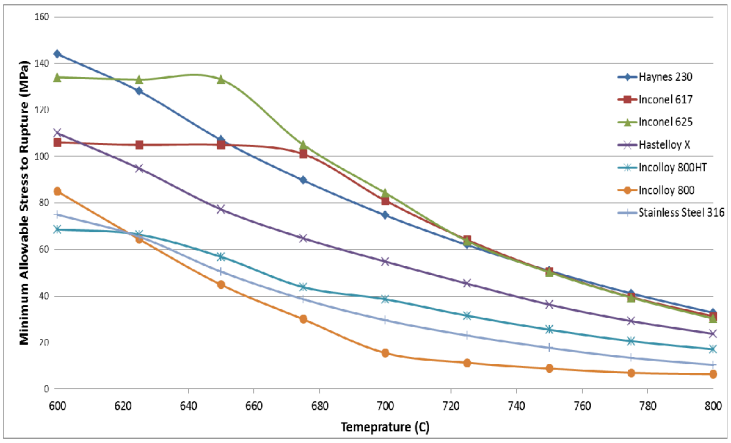

Dostal et al. shows that the receiver outlet pressures on the order of 20-25 MPa and outlet temperatures on the order of 650-700°C are expected in order to achieve a 50% thermal efficiency [6]. Therefore, the tubular receivers that employ sCO_2 as the heat transfer fluid require tubes with a small diameter that can sustain the high working pressure required to maintain the supercritical phase.

Tube Selection

Tube size and wall thickness were selected to maximize heat transfer while minimizing pumping losses. The internal heat transfer coefficient scales as the inverse of the diameter, making small diameters attractive for convective heat transfer. Equation 1 is *ASME Pressure Piping B31.1 Code* design equation for pressurized tubes and pipes, and it was used to select the optimal tube thickness and outside diameter.

$$t = \frac{P \cdot O.D.}{2(S \cdot E + P \cdot y)} \quad (1)$$

Where t is the minimum thickness required excluding manufacturing tolerance and allowances for corrosion, P is the working pressure, $O.D.$ is the external diameter, S is the maximum allowable stress at working temperature, E is the joint efficiency factor, and y is the temperature coefficient. For Nickel-alloys y=0.7 at temperatures above 650°C, while for seamless tubes E=1. Figure 2a and 2b show the required wall thickness for a given outside diameter at isothermal 750°C tube temperature with 20 and 25 MPa of internal pressure, respectively. For practical purposes, 750°C will be the maximum temperature allowed since the maximum allowable stress is on the order of 50 MPa. The diameter chosen should be 12.7 mm in order to have the smallest wall thickness, in this case of 2.324 mm for 25 MPa.

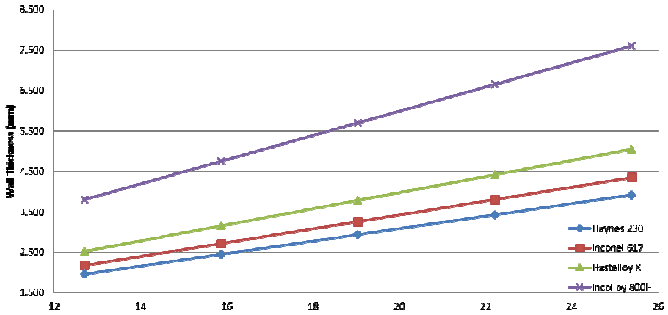

Figure 1: Maximum allowable stresses as a function of temperature. These values correspond to the 80% of the minimum creep rupture stress at 100,000 hours [17].

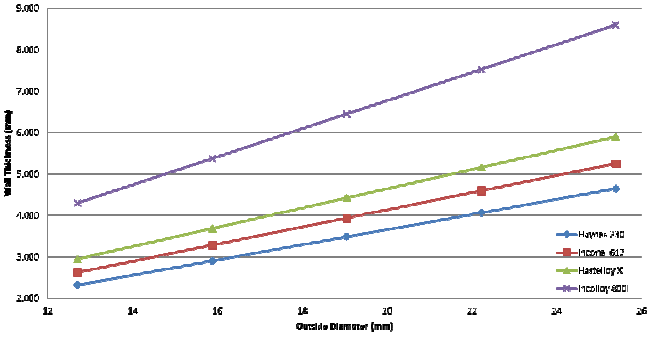

Figure 2: Minimum wall thickness for tubes made from different alloys with similar O.D. at 750°C and a) 20 MPa and b) 25 MPa of constant internal pressure.

Cao and Anderson Et al. measured the weight change of a Haynes 230 coupon exposed to sCO_2 at 650°C and 20.4 MPa as a function of time [18]. Equation 2 is the empirical correlation that describes the change in weight per unit area of the Haynes 230 sample.

$$\Delta W = 0.012t^{0.32} \quad (2)$$

where ΔW is the change of weight in grams per unit area (g/cm^2), and t is the time in hours. Equation 3 is used to estimate the material loss of the sample.

$$ML = \frac{\Delta W}{\rho} \quad (3)$$

where ML is the metal loss (cm), ΔW is the change of weight in grams per unit area (g/cm^2), and ρ is the Haynes 230 density in (g/cm^3).

The estimated material loss for 100,000 of operation is approximately 0.5325 mm. This value will be added to the previous thicknesses calculated. From this we obtain the first set of dimensions, an outside diameter of 12.7 mm and an estimated wall thickness of 2.8565 mm. Since the nearest standard tube sizes were 2.7686 mm (0.109'') and 3.048 mm (0.12''), the first value of 2.7686 mm was selected since the thickness calculated from equation does not consider the different loading conditions which are different during operation and non-operational time. Also, the thickness estimated wall thickness is obtained under the assumption of a maximum surface temperature of 750°C, which is not desired.

Moreover, CSP receiver tubes are always subjected to a radial temperature gradient between the outer and inner walls of the tube. At steady-state, the heat transfer rate and the thermally-induced stresses across the tube-walls are proportional to the wall-temperature difference [1]. More than a radial thermal gradient, a non-axisymmetric radiant heating will produce radial, tangential and axial temperature gradients along the surface of the tube. The two main drawbacks of using the code exclusively and without any modifications inclined to CSP applications:

1. Although *Section I* considers the design of power boilers and superheaters, it is mainly design for power plants which typically are convectively heated by flue gas at relatively low rates of thermal flux.
2. The large safety requirements developed for nuclear components in *Section III, Division I – Subsection NH* will require further simplifications since the level of conservatism in the creep-fatigue analyses is not necessary for CSP applications [17].

Aside from analyses required to design for the resulting stresses due to the thermal and pressure loads, the tubular receivers experience fatigue and creep damage accumulation which will produce failure. Since CSP receivers operate diurnally, they experience a significant cyclical behavior which accumulates fatigue damage on the tubes. Additionally, in order to achieve the required outlet temperatures, the receivers will need to operate at temperatures higher than 40% of the absolute melting point, which is the typical point where creep damage becomes relevant in design.

In order to account for this accumulated damage, a set of simplified design rules based on the nuclear code were developed for CSP receivers were documented in an interim design standard for solar energy applications (SAND79-8183). This approach simplifies the design methodology for a creep-fatigue analysis with a cumulative damage approach [16].

$$\sum_{j=1}^{p}\left(\frac{n}{N_d}\right)_j + \sum_{k=1}^{q}\left(\frac{t}{T_d}\right)_k \leq D \quad (4)$$

The general creep-fatigue damage equation for p number of unique loading cycles, and q number of unique creep loads, where N_d is the number of allowable and n is the number of applied cycles at known loading cycle j, T_d is the allowable creep rupture time and t is the applied load time at loading condition k. Grossman et al. [19] highlights that this creep-fatigue analysis is based entirely on test data and not on the specific processes leading to creep-fatigue failure. Therefore, D, the total allowable accumulated damage is a material property and varies between alloys. Reference material for Haynes 230 suggests that $D \approx 1.0$ [20].

As mentioned by Neises et al. 10,000 cycles, equivalent to 240,000 hours of load time, were assumed to model approximately 30 years of service life [1]. Approximately 100,000 hours are operational time and 140,000 hours are non-

operational time. Starting and shutting down times are considered transient periods which require more detailed analyses and are not considered in this work.

MODEL VALIDATION

The procedure followed was presented by Neises et al. [1] which focuses on the development of an analytical model using the pressurized cylinder equations. The calculated stress components throughout the tube are calculated analytically. Each component is composed of the mechanical and thermal stresses which are resulting stresses from the pressure and thermal load respectively. The results obtained from the analytical models were then used to build a finite element analysis (FEA) structural model using ANSYS Mechanical.

Boundary Conditions

Tables 1 and 2 show the boundary condition parameters used in the FEA structural model. Figure 3 and 4 show the boundary conditions used in the FEA model as shown in tables 1 and 2. The thermal distribution was obtained from ANSYS Fluent using constant temperature inner and outer walls. Both ends of the tube were allowed to freely expand by specifying a weak springs boundary condition.

Parameter	Value (Units)
O.D./Thickness	12.7/2.7686 (mm)
I.D./O.D. Temperatures	737.15/740.06 (^{o}C)
Internal Pressures	20 (MPa)
E (Young's Modulus)	164 x10^{3} (MPa)
α (thermal expansion coefficient)	17.1 x10^{-6} (1/^{o}C)
ν (Poisson's ratio)	0.31 (-)

Table 1: Parameters used as for 20 MPa and 700^{o}C outlet pressure and temperature. (Case 1)

Parameter	Value (Units)
O.D./Thickness	12.7/2.7686 (mm)
I.D./O.D. Temperatures	687.15/695.65 (^{o}C)
Internal Pressures	25 (MPa)
E (Young's Modulus)	168 x10^{3} (MPa)
α (thermal expansion coefficient)	16.8 x10^{-6} (1/^{o}C)
ν (Poisson's ratio)	0.31 (-)

Table 2: Parameters used as for 25 MPa and 650^{o}C outlet pressure and temperature. (Case 2)

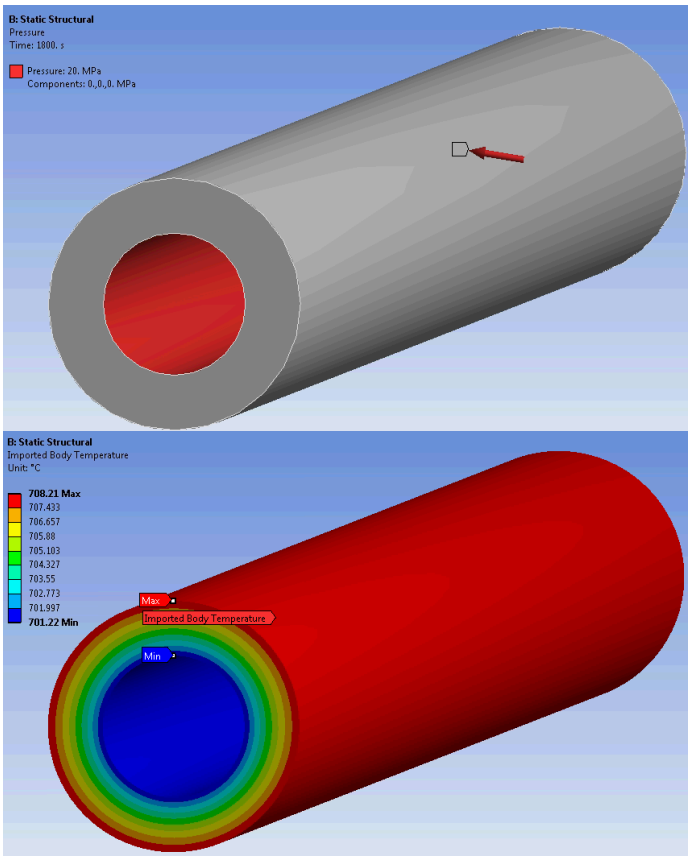

Figure 3: Boundary conditions applied for 20 MPa and 700^{o}C outlet pressure and temperature. (Case 1)

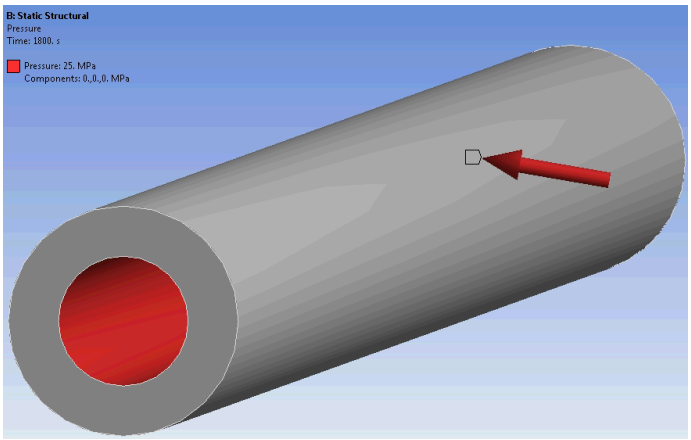

Figure 5: Mesh used for the FEA structural modeling.

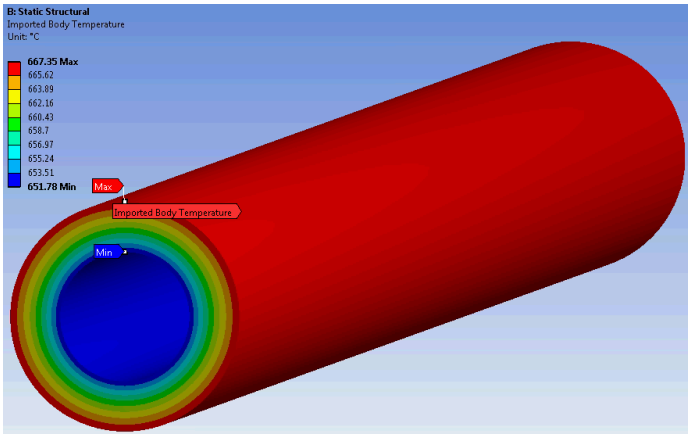

Figure 4: Boundary conditions applied for 25 MPa and 650°C outlet pressure and temperature. (Case 2)

Mesh Independence

A mesh independence analysis was performed using case 1. The goal of the mesh independence analysis was to obtain a percent difference below 1% between the FEA and the Analytical maximum stress levels. An edge size of 1 mm and 3 divisions yielding ~350k elements was selected as shown in figure 5.

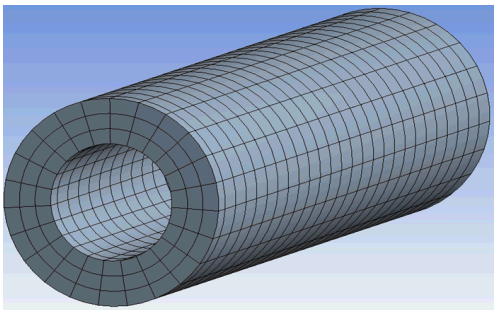

Model Validation

A static structural stress analysis was performed in order to understand the stress distributions across the tube and estimate the life of a tube that undergoes the loads described in the boundary condition section. Figures 6 to 9 display the stress gradient across the tube wall due to the applied mechanical and thermal loads. The analytical stresses in figure 6 and 8 were calculated using the method presented by Neises et al., [1]. As mentioned by Neises Et al., it can be observed that the inner wall of the tube is the most important section of the tube at these high temperatures and pressures [1]. Therefore, the section of focus will be the inner wall for the rest of the study.

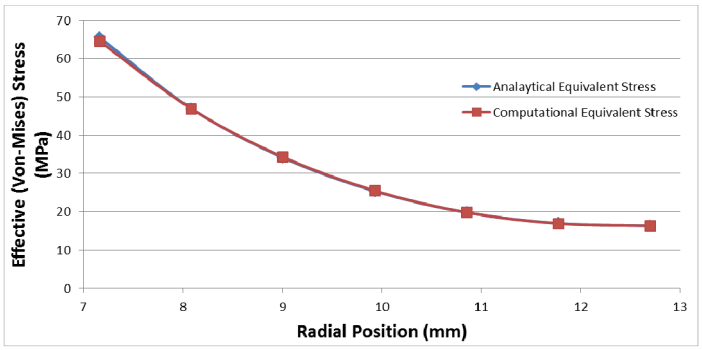

Figure 6: Equivalent stress ($\bar{\sigma}_{eff}$) distribution do to the internal pressure of 20 MPa and temperature difference (Case 1).

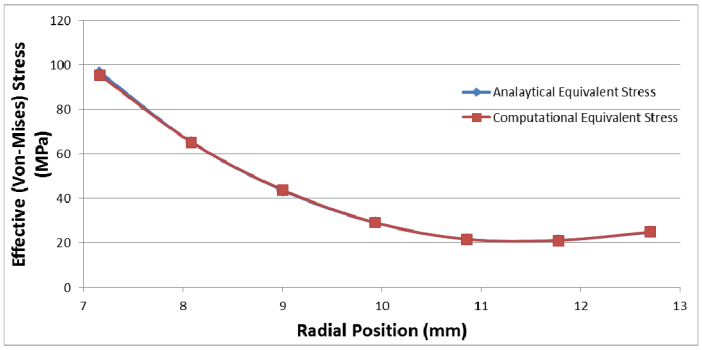

Figure 7: Equivalent stress ($\bar{\sigma}_{eff}$) distribution do to the internal pressure of 25 MPa and temperature difference (Case 2).

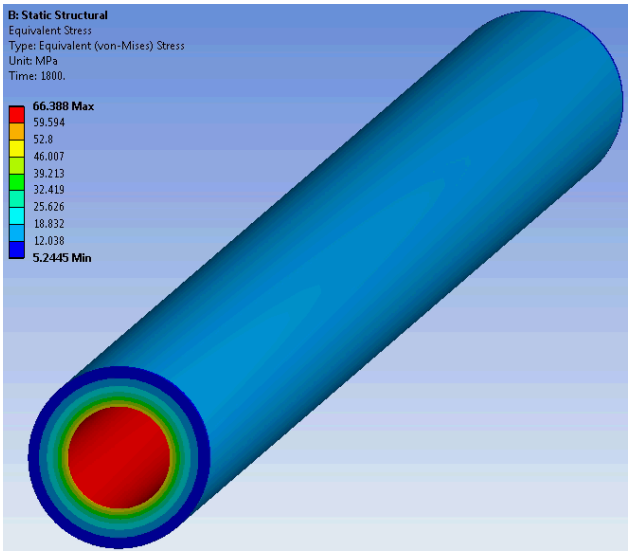

Figure 8: Stress distribution do to the internal pressure of 20 MPa and temperature difference (Case 1).

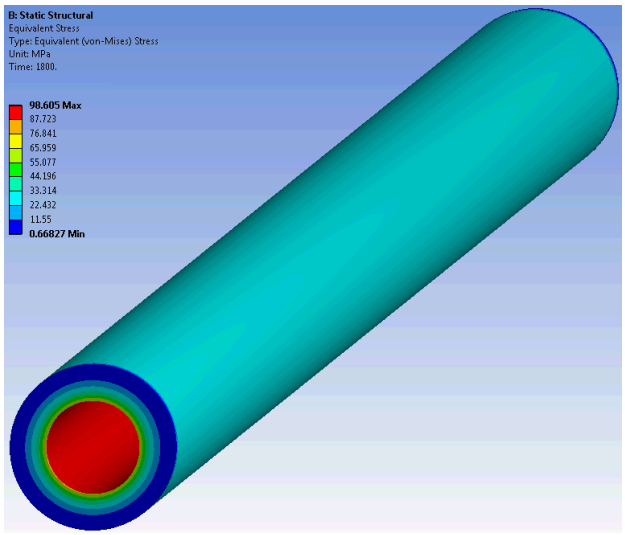

Figure 9: Equivalent Stress (σ_{eff}) distribution due to the internal pressure of 25 MPa and temperature difference (Case 2).

It can be observed that the values of the analytical and computational analyses are comparable in magnitude and follow the same type of distribution. The static structural analyses were validated with the analytical calculations. As a result, a more representative thermal-structural model can be performed by coupling a non-axisymmetric temperature distribution more representative from a tubular receiver, which is the ultimate goal of this work. Another important remark is that the stress concentrations for case 2 are higher. This is because the number of tubes required in both cases is different in order to maintain the same analytical accumulated damage from equation 4. 1150 tubes are required for case 1 while 460 for case 2 in order to meet the requirement of $D \leq 1$. This is because the creep damage is a function of the reciprocal of the absolute temperature T and the logarithmic stress $log(\sigma)$. Therefore, case 2 was chosen to be more appropriate for the rest of this work.

THERMAL-STRUCTURAL MODELING RESULTS

A static thermal-structural analysis is a type of finite element analysis (FEA) that couples the thermal solution or temperature distribution and numerically approximates the resulting stress distributions throughout a designed part. These stress levels are used to estimate the creep-fatigue accumulated damage using the same methodology used by Neises et al [1]. Ortega et al. has published an analogous work containing the results of a coupled optical-thermal-fluid modeling analysis performed using ANSYS Fluent to evaluate the temperature distribution and absorption efficiency of the tubes of tubular receiver [21].

Boundary Conditions

While the internal pressure was kept constant at 25 MPa, the temperature distribution was obtained from Ortega et al. [21] while coupling the optical-thermal-fluid temperature distributions throughout the tube using ANSYS Fluent with ANSYS Mechanical. Figures 10a and 10b shows the temperature distributions applied on the tube surface.

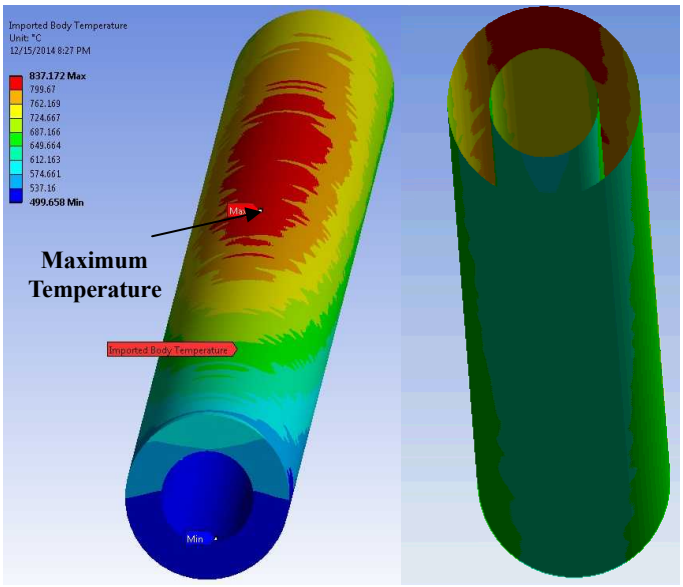

Figure 10: a) Temperature distribution along the tube for ~700 kW/m^2 and b) temperature distribution along the tube with a cross-sectional cut along the region with highest temperature.

From figure 10b it can be observed that the highest inner wall temperature is ~700°C which would be used to approximate the creep damage on the inner wall, being the region of interest.

Stress and Strain Distributions

Figures 11a, 11b, and 11c show the stress and strain distributions which will be used to approximate the fatigue-creep accumulated damage. As expected, the highest stresses are located on the inner walls of the tube which was the area of interest. There are two points of interest on the inner surface of the tube.

- Front side: Displays lowest stress levels but highest temperature.
- Back side: Displays highest stress levels but lowest temperature.

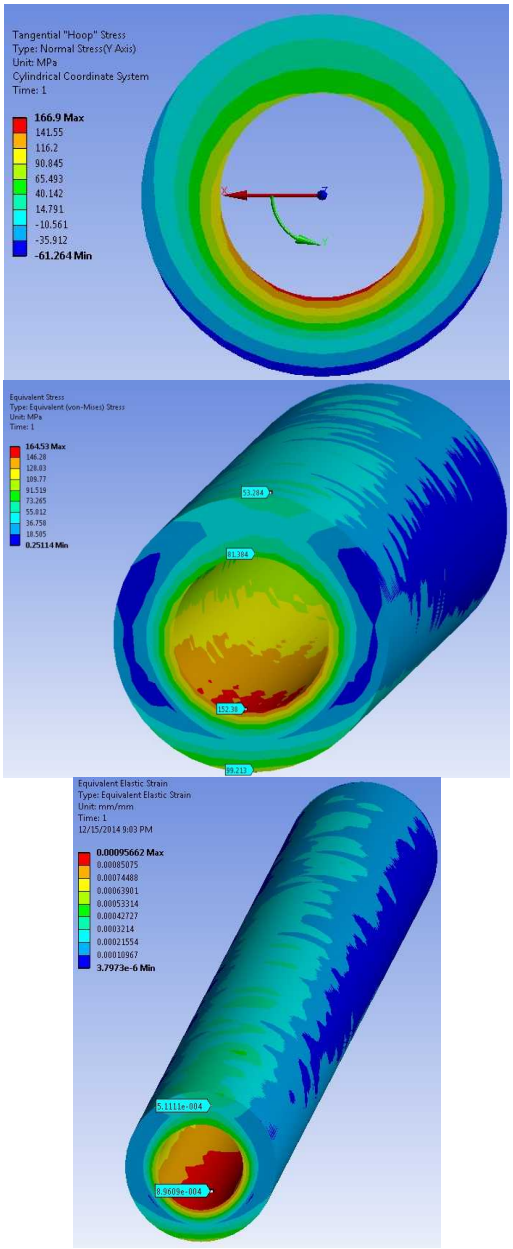

Figure 11: a) Tangential "Hoop" stress distribution, b) Equivalent stress distribution, and c) Equivalent strain distribution along the tube with a cross-sectional cut along the region with highest temperature.

Fatigue and Creep Accumulated Damage

Using the elastic strain values obtained from the analysis on figure 11c and the graph shown in figure 12, the number of cycles to failure can be estimated. It can be observed that both cases have an elastic strain that is low enough to consider fatigue damage negligible. Although the number of cycles to failure is high, Neises Et al. suggests fixing the value of the fatigue accumulated damage to 0.1 as an added safety factor [1].

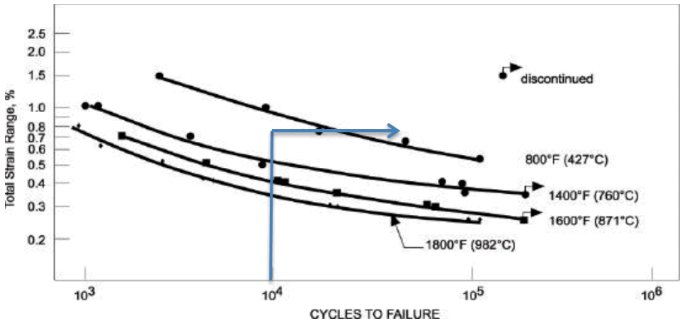

Figure 12: Total Strain Range vs Cycles to Failure of Haynes 230 [22]. The blue arrow marks the minimum required number of cycles.

Eno et al. [23] published a several methods that use equation 5 to extrapolate the rupture time of Haynes 230. The method expresses the logarithmic time, log(t), as a function of the reciprocal of the absolute temperature T and logarithmic stress, log(σ) as shown in equation 5.

$$\log(t) = \beta_0 + \beta_1 \frac{1}{T} + \beta_2 \log(\sigma) + \beta_3 \log(\sigma) \frac{1}{T} \quad (5)$$

The four coefficients were empirically based on the creep data from Haynes [24]. Table 3 shows the parameters presented by Eno et al. for a 95-percentile Mendelson-Roberts-Manson (M-R-M) creep mode, which is a variation of the commonly used Larson-Miller creep model. Table 4 shows the temperature and stress levels at the points of interest previously described.

Point of interest	Temperature (K)	Equivalent Stress (MPa)
Front	993.15	81.15
Back	863.15	152.4

Table 4: Temperature and stress levels at the points of interest.

As mentioned before, 10,000 cycles are equivalent to 240,000 hours of service life. Approximately 100,000 hours are operational time and 140,000 hours are non-operational time. Starting and shutting down times are considered transient periods which require more detailed analyses and are not considered in this work. During the stand-by period, the pressure is maintained and the temperature cools down to ambient temperature. The rupture time was found to be ~1.3×10^{62} hours, which makes the accumulated damage during the stand-by period negligible for the calculations. Table 5 displays the accumulated damage calculations using equation 4.

Point of interest	Allowable creep rupture time (Inner Wall) (hrs.) T_d	Creep Damage (Inner Wall) t/T_d	Fatigue Damage (Inner Wall) n/N_d	Total Damage (Inner Wall) D
Front	109,525	0.913	0.1	**1.013**
Back	1.246×10^7	0.008	0.1	**0.108**

Table 5: Total damage calculated from equation 4 as the result of the temperature and equivalent stress at the points of

In table 4, it can be observed that the front part of the inner wall of the tube has lower stress levels compared to the back part. This can be attributed to the uneven thermal expansion rates, at different points throughout the tube, due to the thermal gradient. From a structural point of view, this stress distribution could be beneficial, because the higher stress concentrations will be occur in regions where the temperature is lower and the material can easily withstand those stress levels. These creep-fatigue values are being corroborated with nCode Design Life using the Larson-Miller creep model for a more detailed work-life estimate.

CONCLUSIONS

By completing this work, the possibility of a high temperature and high pressure supercritical carbon dioxide has been confirmed.

The static structural FEA was validated using the analytical formulations presented. As a result, a more complex thermal-structural FEA was performed. This method allows the designer to focus on the weaker sections of the receiver and adjust accordingly to the concentration levels that the receiver will be exposed to. This new method of coupling will help to estimate the life of the new generation of solar thermal receiver.

Currently, there are no other published studies analogous to this one. This work will serve as reference for future design and evaluation of future direct and indirect tubular receivers.

This methodology is geometry independent, so any type of structures could be analyzed by applying the corresponding boundary conditions and constraining the analyses appropriately.

ACKNOWLEDGMENTS

This research is based upon work supported by the Solar Energy Research Institute for India and the U.S. (SERIIUS) funded jointly by the U.S. Department of Energy subcontract DE AC36-08G028308 (Office of Science, Office of Basic Energy Sciences, and Energy Efficiency and Renewable Energy, Solar Energy Technology Program, with support from the Office of International Affairs) and the Government of India subcontract IUSSTF/JCERDC-SERIIUS/2012 dated 22nd Nov. 2012.

REFERENCES

1. **T. W. Neises, M. J. Wagner, A. K. Gray**, *Structural Design Considerations for Tubular Power Tower Receivers operating at 650 C,* Proceedings of the 8th International Conference on Energy Sustainability (ES2014), Boston, MA, June 30th – July 2nd 2014, ASME Paper No. 6603.

2. **Romero M, Buck R, Pacheco J E.,** An update on solar central receiver systems, projects, and technologies. J Solar Energy Eng 2002;124:98e108.

3. **Li X, Kong W, Wang Z, Chang C, Bai F.,** Thermal model and thermodynamic performance of molten salt cavity receiver. Renew Energy 2010;35:981e8.

4. **Burgaleta JI, Arias S, Ramirez D., Gemasolar, the** first tower thermosolar commercial plant with molten salt storage. In: Proceedings of the Solar PACES 2011 conference on concentrating solar power and chemical energy systems. Granada, Spain 2011.

5.**Yu Q, Wang Z, Xu E, Li X, Guo M.,** Modeling and dynamic simulation of the collector and receiver system of 1MWe DAHAN solar thermal power tower plant. Renew Energy 2012;43:18e29.

6. **Dostal V.**, "A supercritical carbon dioxide cycle for next generation nuclear reactors," PhD Thesis, Nuclear Engineering, (2004) Massachusetts Institute of Technology.

7. **Seidel W.**, "Model developmenet and annual simulation of the supercritical carbon dioxide Brayton cycle for concentrating solar power applications," Master of Science Thesis, Mechanical Engineering, (2010) University of Wisconsin-Madison.

8. **Angelino G.**, "Carbon dioxide condensation cycles for power production," Journal of Engineering for Power, 90 (1968) 287-296.

10. **Dostal V., Hejzlar P. and Driscoll M. J.**, "High-performance supercritical carbon dioxide cycle for next-generation nuclear reactors," Nuclear Technology, 154 (2006) 265-282.

11. **Moisseytsev A. and Sienicki J. J.**, "Extension of supercritical carbon dioxide Brayton cycle for application to the very high temperature reactor," International Congress on the Advances in Nuclear Power Plants (2010) San Diego, CA, June 13-17, 2010.

12. **Angelino G.**, "Real gas effects in carbon dioxide cycles," ASME International Gas Turbine Conference and Products Show GT-102 (1969) Cleveland, OH, March 10-13, 1969.

13. **Dostal V., Hejzlar P. and Driscoll M. J.**, "The supercritical carbon dioxide power cycle: Comparison to other advanced power cycles," Nuclear Technology, 154 (2006) 283-301.

14. **Turchi C. S.**, "Supercritical CO2 for application in concentrating solar power systems," sCO2 Power Cycle Symposium (2009) Troy, NY, April 29-30, 2009.

15. **Glatzmaier G. C. and Turchi C. S.**, "Supercritical CO2 as a heat transfer and power cycle fluid for CSP systems," ASME Energy Sustainability (2009) San Francisco, CA, July 19-23, 2009, pp. 673-676.

16. **I. Berman, A. C. Gangadharan, G. D. Gupta, and T. V. Narayanan**, *An Interim Structural Design Standard for Solar Energy Applications*, Sandia National Laboratories, Livermore, CA, Report No. SAND79-8183, 1979.

17. *ASME Boiler and Pressure Vessel Code*. New York, NY: American Society of Mechanical Engineers, 2013

18. **G. Cao, M. Anderson, K. Sridharan, L. Tan, T. Allen**, *Corrosion of Candidate Alloys in Supercritical Carbon Dioxide*, University of Wisconsin-Madison, pg. 1-28.

19. **J. W. Grossman, W. B. Jones, and P. S. Veers**, *Evaluation of Thermal Cycling Creep-Fatigue Damage for a Molten Salt Receiver,* 12th Annual ASME International Solar Energy Conference, 1990.

20. **X. Chen, M. a. Sokolov, S. Sham, D. L. Erdman III, J. T. Busby, K. Mo, and J. F. Stubbins**, *Experimental and modeling results of creep–fatigue life of Inconel 617 and Haynes 230 at 850°C.*, J. Nucl. Mater. vol. 432, no. 1–3, pp. 94–101, Jan. 2013.

21. **J. D. Ortega, S. D. Khivsara, J. M. Christian, J. E. Yellowhair, C. K. Ho**, *Coupled Optical-Thermal-Fluid Modeling of a Directly Heated Tubular Solar Receiver for Supercritical CO2 Brayton Cycle,* Proceedings of the 9th International Conference on Energy Sustainability (ES2015), San Diego,CA, June 28th – July 2nd 2015, *To be published.*

22. *Haynes 230 Alloy*, Haynes International http://haynesintl.com

23. **Eno, D. R., Young, G. A., and Sham, T.-L.**, 2008, *A Unified View of Engineering Creep Parameters*, Proceedings of ASME Pressure Vessels and Piping Division Conference (PVP2008), Chicago, July 27–31, ASME Paper No. 61129, pp. 777–792.

24. *Haynes 230 Creep Data Spreadsheet*, Haynes International http://haynesintl.com